Vibration Durability Investigation for SAC and SnPb Solder: Based on JCAA/JG-PP Lead-Free Solder Project Test Results

Abstract:

The main objective of this report is to use a Physics of Failure (PoF) based approach for accelerated qualification of both Sn3.9Ag0.6Cu (SAC) and Sn37Pb (SnPb) assemblies, under vibration loading. The test data for this qualification, available from the JCAA/JG-PP Lead-Free Solder Project test program, includes the characteristic strain histories at specific locations on the JG-PP "pathfinder" PWA and the durability life data for both SAC and SnPb assemblies. Corresponding simulation work for this test article is conducted at CALCE. The simulation results, in conjunction with the experimental results, are used to verify the slopes of the fatigue S-N curves for vibration durability of both SAC and SnPb solders. The model results are compared with test results to verify the effect of the component location on the PWB and also the effect of the excitation levels.

Specifically, results of the following tasks are presented in this report:

1. Global FEA of the circuit card assembly used in the JGPP test program to simulate modal response and strain response under random vibration excitation.
2. Detailed local FEA of selected components to investigate stress-strain history in the solder interconnect.
3. Normalized durability ranking of various SAC and SnPb BGA

interconnects. Simulation results and available solder fatigue data were used to verify the exponents of the power-law durability models.

4. Demonstration of acceleration curves for one selected BGA component.

Revision History

Contributor	Date	Description
Y. Zhou & A. Dasgupta	08/17/2006	First Draft
Y. Zhou & A. Dasgupta	10/27/06	Second Draft

Reviewed and Approved: __ 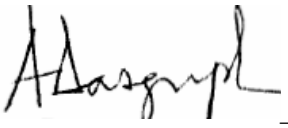 _____ _____10/27/06_____
(signature) (date)

Content Disclaimer

The information contained in this document is designed to be accurate and authoritative in regards to the subject matter covered. However, it is provided with the understanding that the provider is not engaged in rendering legal, accounting, engineering, or other professional services. It is intended to be used for educational purposes only. CALCE Electronic Products and Systems Center (EPSC) disclaims any responsibility or liability for this material and is not responsible for the use of this information outside of its educational purpose.

Copyright Notice

The information contained within this packet has been developed by the
University of Maryland, CALCE Electronic Products and Systems Center (EPSC).

Replication rights of all information is retained by the
CALCE Electronic Products and Systems Center.

Copyright © 2003 CALCE EPSC and the University of Maryland. All rights reserved.
Accelerated Qualification of Pb-free Electronic Assemblies

1. Introduction and Problem Statement

Vibration loading is commonly encountered in the service life of electronic packaging and its contribution to fatigue damage accumulation in solder interconnects must also be investigated. The characteristics of the stress from vibration loading are low amplitude and high accumulating rate. A lot of work has been conducted for vibration durability investigation. K. Darbha [1] investigated stress distribution of surface mount interconnections due to vibration loading. Barker et al. [2], [3] proposed some analytical methods to estimate the vibration fatigue lives of leaded surface mount components. Liguore et al. [4] developed a simple vibration fatigue life prediction technique for the LLCC solder joints. Lau et al. conducted vibration reliability testing [5] [6] [7] using sweep sinusoidal excitations and studied vibration fatigue properties based on linear assumption. Q. J. Yang [8] investigated the reliability of a PBGA assembly under a sinusoidal excitation. In his study, the dynamic displacement of the PBGA assembly was found to be highly nonlinear under the out-of-plane excitation. Most failures were due to cracks near the copper pad on the PCB side in Q. J. Yang's [8] work. F.X. Che [9] conducted fatigue tests and analysis for flip chip solder joint under sinusoidal sweep test with a narrow band near the fundamental resonant frequency.

As part of the JCAA/JG-PP Lead-Free Solder Project, accelerated vibration durability tests were conducted on both Sn3.9Ag0.6Cu (SAC) and Sn37Pb (SnPb) circuit card assemblies, using broad-band random step stress excitation [10]. The test vehicle is shown in Figure 1.

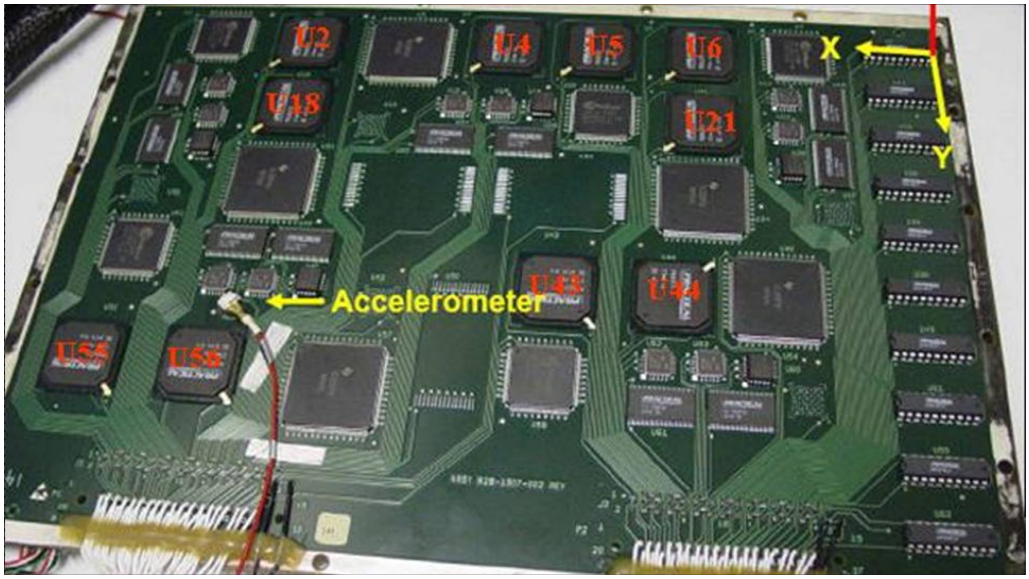

Figure 1: JGPP "pathfinder" test vehicle and locations of BGA components

In this report, Physics of Failure (PoF) analysis is conducted on the ten BGA225 components, shown in Figure 1, to compare the vibration durability and acceleration factors of SAC assemblies vs their SnPb counterparts.

2. Overall Approach

A time-domain approach, reported in the literature [11], is adapted for this study. The flow chart of this approach is shown in Figure 2.

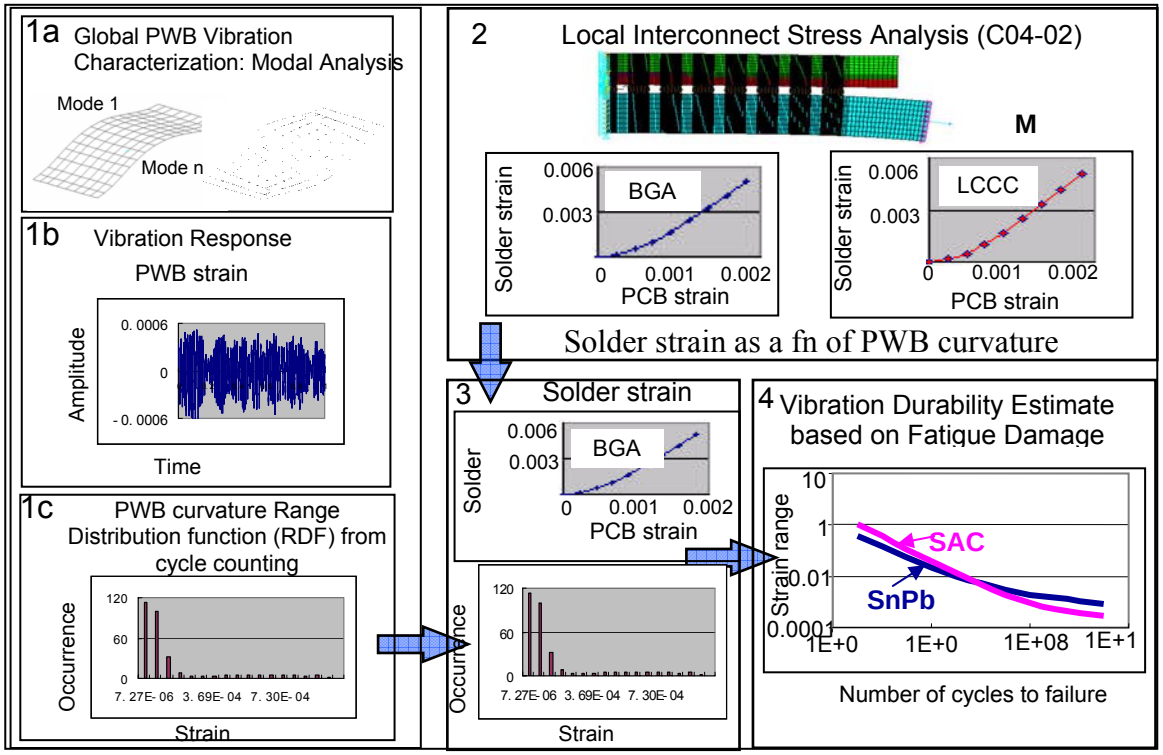

Figure 2: Flow chart of whole vibration time-domain durability approach

The tasks in this approach can be roughly divided into four categories, which are shown in four boxes, respectively.

- **PWB characterization**: Both experiments and FEA simulation are carried out to characterize the dynamic response of the test PWA. Response characterization mainly includes modal analysis and dynamic strain history collection on the test vehicle. Modal characterization is depicted in box 1a. The natural frequencies and corresponding mode shapes of the boards can be obtained here. Corresponding FEA is conducted and calibrated, based on this experiment result. The characteristic flexural strain at different locations on the test board can then be either measured with gages or estimated from the FEA model, under different excitation levels. These strain time histories are then used to construct strain range distribution functions (RDFs) of the PWB, based on cycle counting, as shown in Box 1c.
- **Detailed stress-strain analysis of the critical solder joint**: The work described in Box 1 is all conducted at the board level. To assess the durability properties of the solder joint, the corresponding stress-strain history in the solder joint, due to PWB

flexure, needs to be investigated. The detailed local FEA model of a sample BGA component is shown in Box 2. The output of this analysis is the strain transfer function which relates the equivalent strain in the critical solder joint to the local PWB flexural strain near the foot-print of the component.

- **Quantification of strain history in critical solder joint**: The strain transfer functions from the modal analysis and the local FEA models described above are applied to the measured PWB strain history to obtain the strain history in the critical solder joint. Cycle counting techniques are used to obtain the corresponding strain range distribution function (RDF) in the critical solder joint.
- **Durability estimation**: Finally, a cyclic mechanical fatigue durability model is applied to estimate the vibration durability of the solder under the obtained strain RDFs. Conversely, if corresponding failure test data are available, the durability model constants can be estimated based on failure test results, measured PWB strain RDFs, and strain transfer functions obtained from modeling.

The following data are available from the JCAA/JG-PP Lead-Free Solder Project vibration test report [10]:

1. Durability results (time to failure) for all failed components.
2. Flexural strain histories at different excitation levels, from a strain gage at a specified location on the PWB.
3. Fundamental modal frequencies and mode shapes, based on laser vibrometry.

Global FEA of the PWB is first conducted in this study to extrapolate the strain history measured from the strain gage to all locations of interest on the PWB. The locations of interest include the locations of the ten BGA components shown in Figure 1. The modal frequencies and mode shapes predicted by the global FEA model are compared to experimental measurements. Local FEA for the BGA225 component is carried out to obtain strain in the critical solder joint for a given magnitude of PWB flexure. Finally, the experimental durability results are used to calibrate the durability model constants. The calibrated model is then used to compare and rank durability results and acceleration factors for different BGA locations and different solders. The details are described in the following sections.

3. Global FEA for Dynamic Response Characterization of the JGPP Test Vehicle

The circuit card assembly (CCA), used as the JGPP test vehicle, is modeled as a uniform board as shown in Figure 3. The dimensions of the test board are 324 by 228 millimeter and the thickness is 2.28mm. The board is meshed with 1178 shell elements. The PWB material is assumed to behave in a linear isotropic elastic manner in this simulation with a Young's modulus of 17.7 Gpa and Poisson's ratio of 0.39. The card-guide boundary conditions applied to the circuit card assembly along the two short edges at x = 0 mm and x = 324 mm consist of simple translational support in the out-of-plane (z) direction and rotational springs about the y axis.

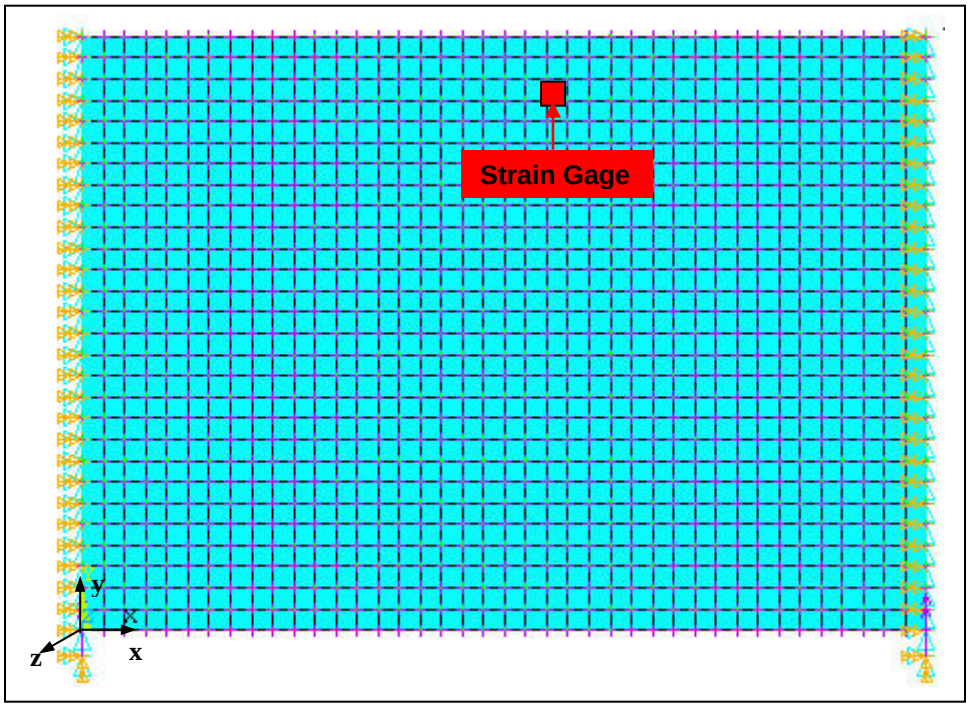

Figure 3: Global FEA model for JGPP test vehicle

The natural frequencies and mode shapes are extracted from the FEA modal analysis and compared with experimental results. The dominant modes from experiment and simulation are compared in Figure 4. The first fundamental natural frequency from experiment is 72Hz. By matching the fundamental natural frequency from simulation, the boundary stiffness for the rotational spring is calibrated to be 9N-m/Rad. Using this rotational spring constant, the simulation results for the remaining mode shapes and natural frequencies are found to agree well with experiment results. The natural frequency of the second dominant mode is 411Hz from experiment and 415Hz from simulation. Simulation and experiment provide the same mode shape for this dominant mode, as shown in Figure 4.

The PSD plots of the strain response show some difference between the experiment and simulation for the magnitude of the 411Hz mode. The strain PSD from simulation is greater than that from experiment. The difference might come from the approximations in our global model. For example, the PWB is modeled as a uniform material although the real circuit card is populated with multiple components. A constant damping ratio is applied to all modes in the simulation. From the mode shape plots, it is clear that the dominant strain component is flexural strain in the x direction.

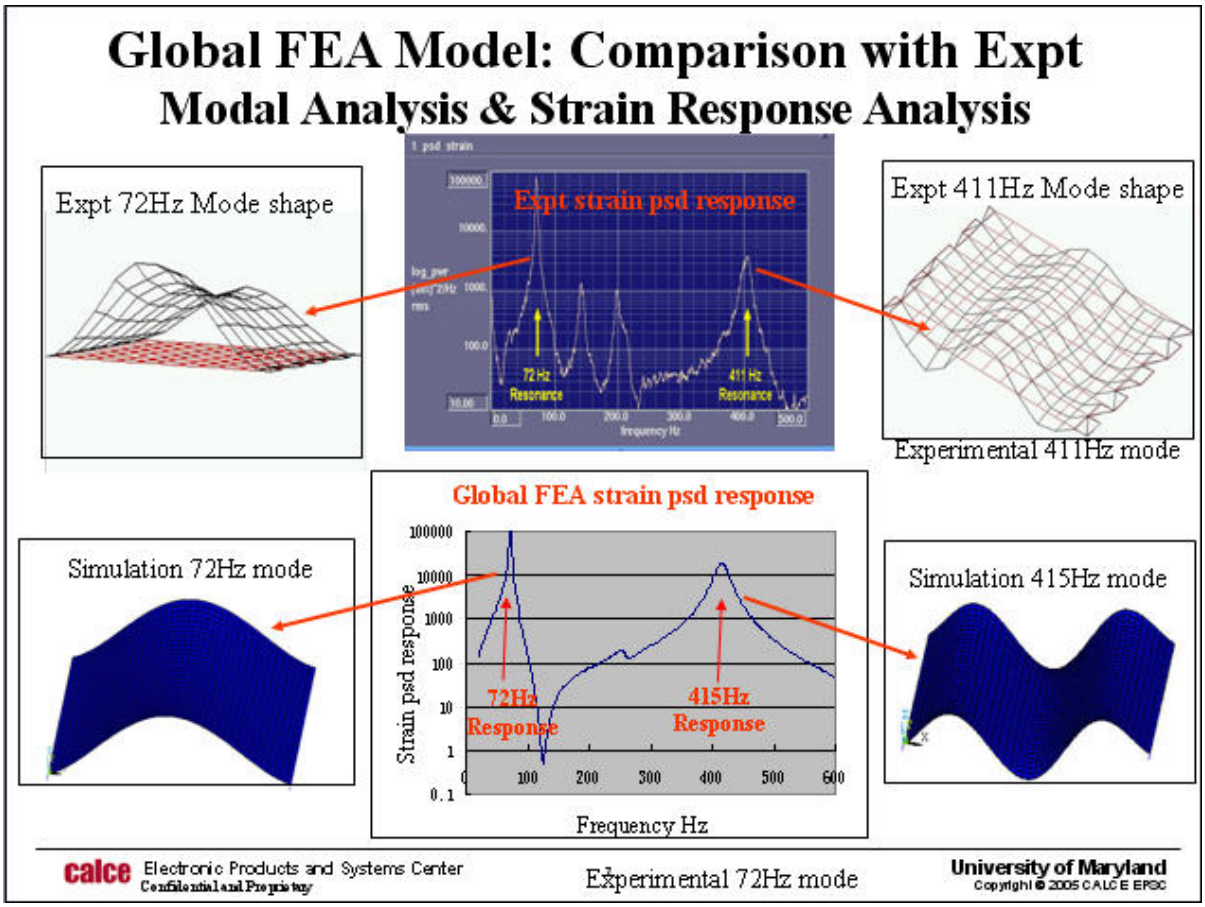

Figure 4: Modal Analysis and strain response results from global FEA and experiment

The strain PSD response from experiment shows that the first mode contributes more than 90% to the total strain response. The broad-band excitation shown in Figure 5**,** ranges from 20Hz to 2000Hz. The global FEA provides an estimate of the corresponding strain response everywhere on the PWB. Figure 6 is a contour plot of the 1-sigma value of the strain variable ε_{xx} obtained from the global FEA of random vibration response. This 1-sigma response is based on the assumption of a Gaussian response to the broad-band excitation.

From the FEA strain response plot, we can calculate the strain scaling factors at the location of each BGA component. The strain scaling factors are defined as the ratio of the strain ε_{xx} in the PWB near each component, to the strain ε_{xx} in the PWB near component U55. The strain values are locally averaged over the length scale of the strain gage characteristic dimensions. U55 is chosen for normalizing all the PWB strain values, since the flexural strain on the PWB is highest near this component. The PWB strain scaling factor results, SSF_{PWB} are listed in Table 1. These scale factors are in qualitative agreement with the laser vibrometry results provided in the JGPP report [10].

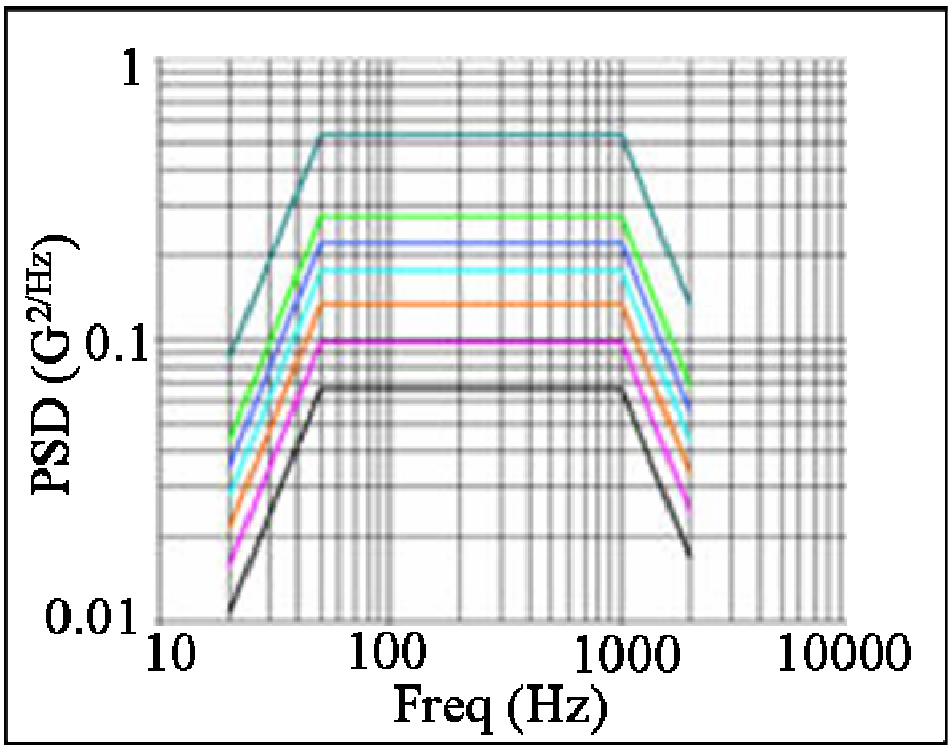

Figure 5: broad-band excitation plot

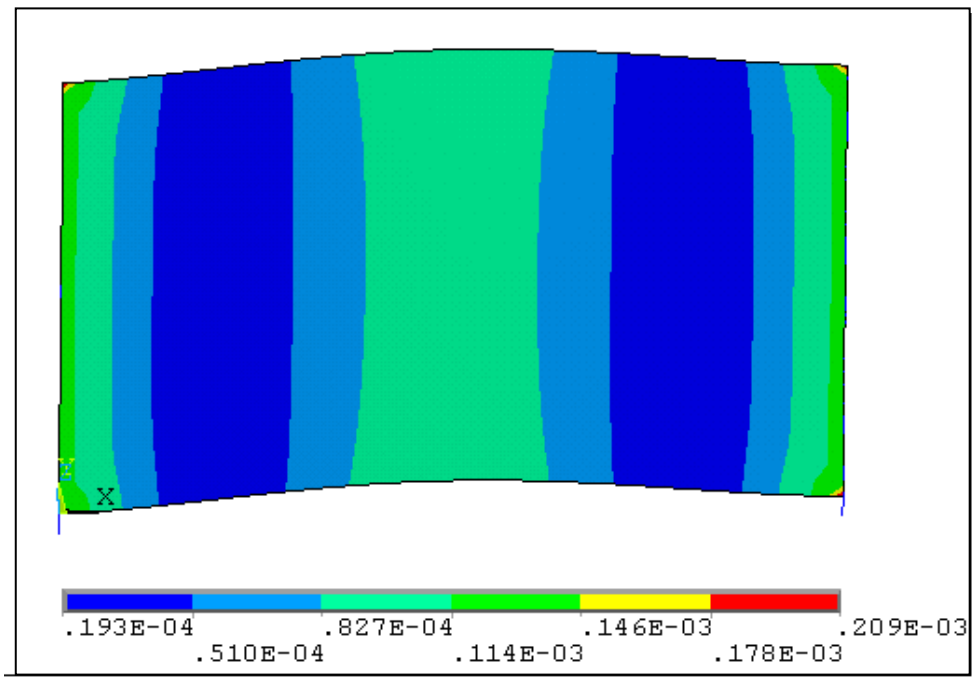

Figure 6: Contour plot for 1σ strain ε_{xx} under 10Grms

U55	U4	U5	U43	U6	U44	U21	U56	U2	U18
1	0.97	0.96	0.85	0.68	0.67	0.63	0.31	0.29	0.27

Table 1: PWB Strain scaling factors for BGA components

In the JGPP experiment, the strain gage is attached near component U4 which has strain scale factor of 0.97**.** With these strain scaling factors, the measured strain from the strain gage can be extrapolated to the site of all components on the entire PWB. Here we take component U55 as an example. As shown in Figure 7, multiplying the strain gage reading (which is also the PWB strain near component U4) by the scaling factor (1/0.97=1.03), the PWB strain history near component U55 can be obtained. The PWB strain histories for other components can be similarly obtained. As discussed in the following section, the PWB strain history near each component is then used to estimate the strain history in the critical solder joint of that component so that the fatigue durability of the solder joint can be assessed.

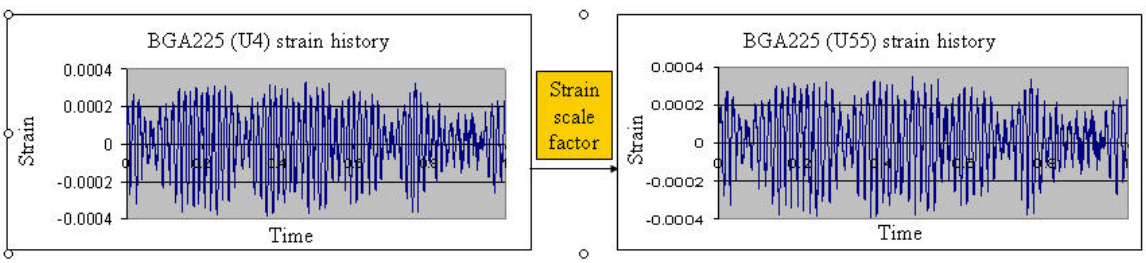

Figure 7: Application of strain scale factor to extrapolate PWB strain history

4. Local Detailed FEA for Stress-Strain Analysis of Solder Joints

After global characterization of the PWB, detailed local finite element analysis is conducted to obtain the strain history in critical solder joints of each component, from the flexural strain history on the PWB near the component. In other words, the purpose of the local FEA is to set up the transfer function between local PWB flexural strain and equivalent strain at the critical location in the critical solder joint. In this report, only BGA255 components are investigated in detail. Two-dimensional models are adequate for this study because the dominant mode shapes have curvatures only in one direction. Only half of the component is modeled because of symmetry. The main dimensions of the model are listed in Table 2. These dimensions are obtained from cross sections and microscope measurements. The material properties for solder, PCB, substrate, die and mold compound are listed in Table 3 and Table 4. Solders are modeled as elastic-plastic materials with power-law hardening. All other materials are modeled as linear elastic.

A bending moment is applied at the edge of the PWB and the resulting deformed shape is shown in Figure 8. The PWB strain is monitored at the nodes along the bottom of the PWB. As shown in Figure 5, the strain gage is attached at the bottom of the PWB, beside the component, where the PWB curvature is highest. The PWB strain is then averaged over the area covered by the strain gage.

	Length (mm)	Height (mm)
PCB	16	2.28
Die	3.75	0.3
Substrate	13.5	0.51
Mold Compound	11	1.184
	Radius (mm)	Height (mm)
Solder	0.5	0.45

Table 2: Dimensions for BGA225 FEA local model

	Young's Modulus (Mpa)	Poisson's Ratio
PCB	17685	0.39
Substrate	4000	0.3
Die	191000	0.278
Mold compound	15900	0.3

Table 3: Material properties [12]

	Young's Modulus (Mpa)	Plastic model	Poisson's Ratio
SnPb	31600	$\gamma_p = 2.34*10^{13}\left(\frac{\tau}{11700}\right)^{5.58}$	0.35
SAC	47500	$\gamma_p = 2*10^{11}\left(\frac{\tau}{17600}\right)^{4.4}$	0.35

Table 4: Material properties for SAC and SnPb solder [13]

From the simulation results, the outer most solder joint is found to be the most critical one. The locally averaged strain at the critical location in the critical solder joint is then calculated. In this study, solder strains are averaged over 2% of the area around the location of maximum strain in the critical solder joint. Finally, the strain transfer functions for both SAC and SnPb solder are obtained from this detailed local FEA, as shown in Figure 9.

Using these global and local FEA results, the strain history in the critical solder joints can now be estimated from the measured PWB strain history. The strain history is collected for a unit time (e.g, 1 second). The procedure is shown in the form of a flowchart, in Figure 10. Here we take component U55 (BGA225) as an example. First the strain history is measured at each excitation level, using the strain gage on the PWB (location was shown in Figure 1). The strain reading is then multiplied by the PWB strain scaling factor from global FEA, in order to obtain the PWB strain near component U55. Then the strain transfer function from local FEA is applied to estimate the strain in the critical solder joint. Finally, solder strain range distribution functions (RDFs) can be obtained, using a cycle counting algorithm. The rain-flow cycle counting technique [14] has been

used in this study. The results are usually averaged over many such time history records.

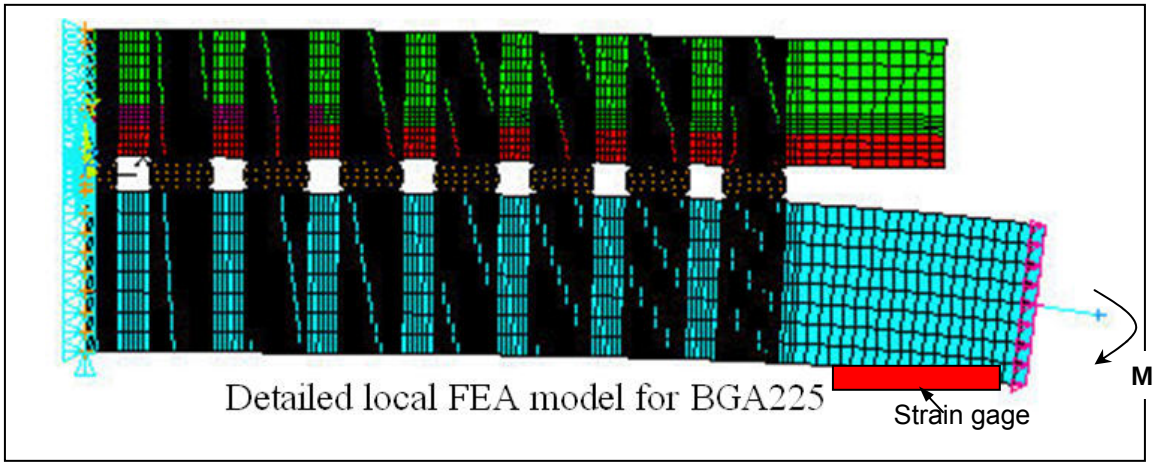

Figure 8: Detailed local FEA model for BGA225 component

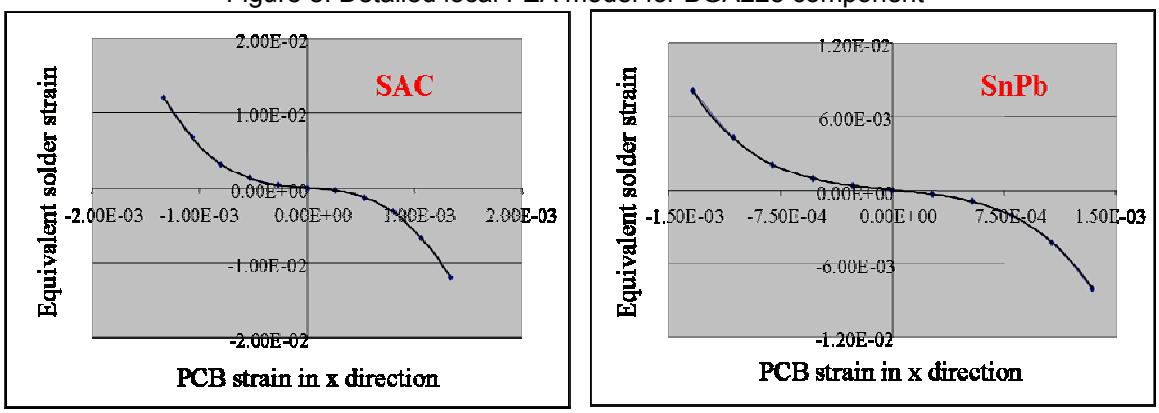

Figure 9: Strain transfer function in BGA225 for both SAC and SnPb from local FEA

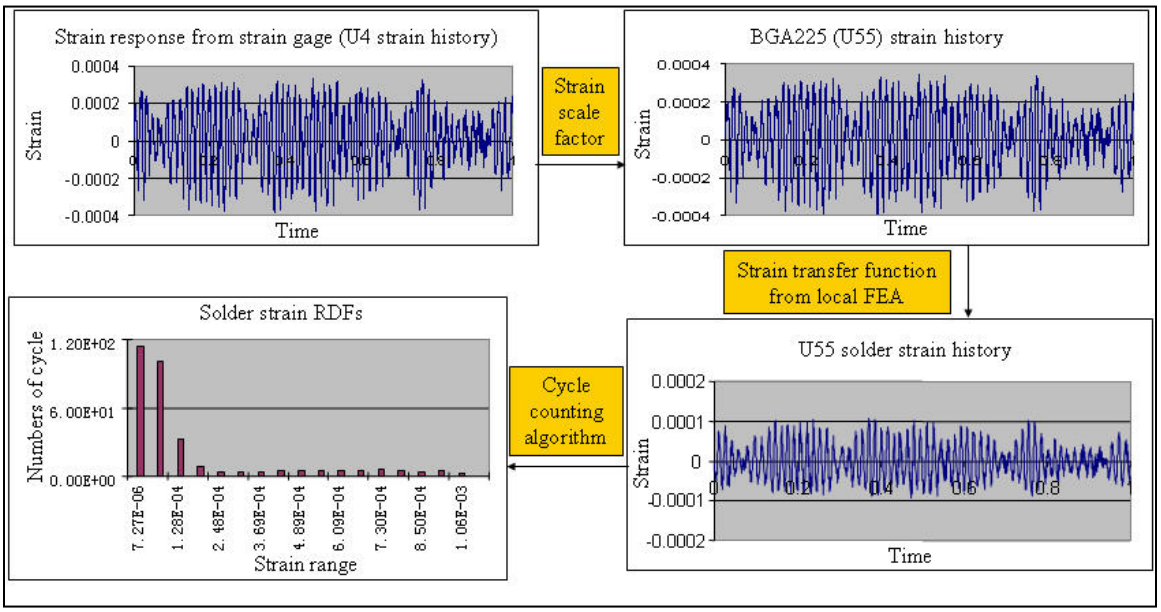

Figure 10: Procedure to obtain solder strain RDFs

5. Durability Scale Factors

This section describes the method for comparing different durability results when step stress excitation is used. As discussed below, the durability results have to be normalized to a common reference excitation level, using a durability scale factor, before comparisons can be made. The durability estimation method for a single excitation level is first described, followed by discussion of the durability scale factor for multi-level strep-stress excitation.

The solder fatigue durability model used in this study is the generalized strain-life Coffin-Manson durability model shown in Equation 2 [14].

$$\frac{\Delta\varepsilon}{2} = \frac{\sigma_f^{'}}{E}\left(2N_f\right)^b + \varepsilon_f^{'}\left(2N_f\right)^c \qquad (2)$$

$\sigma_f^{'}$: Fatigue strength coefficient

$\varepsilon_f^{'}$: Fatigue ductility coefficient

b: Fatigue strength exponent

c: Fatigue ductility exponent

Preliminary fatigue constants for Sn63Pb and Sn3.5Ag0.5Cu solders, estimated from literature [12] [15], are used in this study. The actual values of these constants are available in CALCE consortium databases. Equation 2 is also presented in graphical form, as generalized S-N curves, in Figure 11. Because the model constants are proprietary to the CALCE consortium, the vertical axis in this plot has not been labeled.

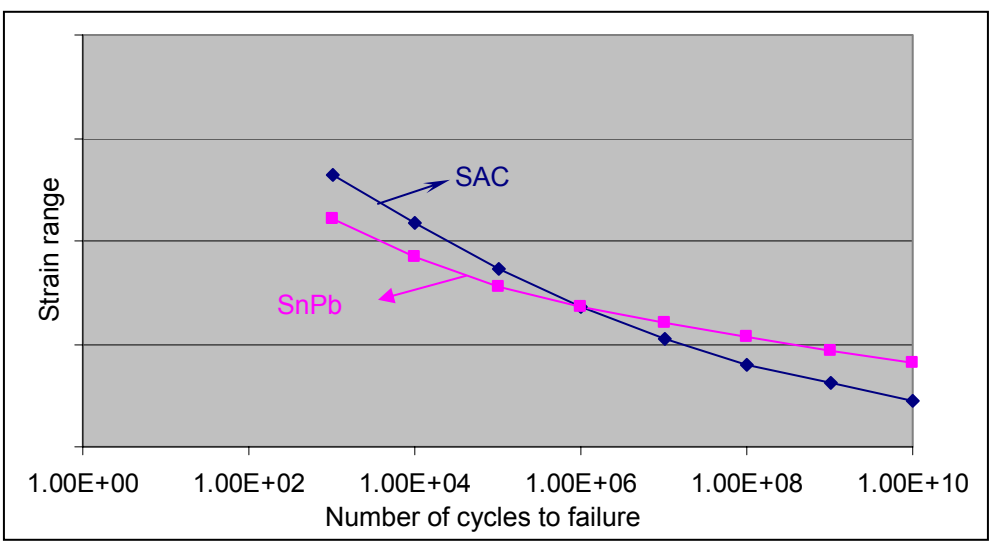

Figure 11: Durability S-N curves for SAC and SnPb

After the cycle counting is conducted in Figure 9 at each excitation level for the strain history at the critical solder joint for record-length of unit time, the corresponding fatigue

damage per unit time is estimated using Equation 2. Equation 2 is applied for each strain level, ε_i, shown on the horizontal axis of the strain RDFs, to obtain the fatigue damage as:

$$D_i = n_{\varepsilon i}/N_{f\varepsilon i} \tag{3}$$

Where n_ε is the number of cycles per second at a given strain level from the RDF and $N_{f\varepsilon}$ is the corresponding cycles to failure at this strain level from Eqn 2 (or Figure 10).

The fatigue damage rate (damage per unit time), $\dot{D}$, is then estimated by summing the damage at each strain level, ε_i, in the RDF, using Miner's linear damage superposition [14].

$$\dot{D} = \sum_i D_i = \sum_i \frac{n_{\varepsilon_i}}{N_{f_{\varepsilon_i}}} \tag{4}$$

The durability (time to failure, t_{f_g}) at excitation level G_{rms} is then obtained as the reciprocal of the damage rate at this excitation level.

The durability assessment in the JGPP study is more complex than the method given in Eqns 1-4, because the JGPP durability test uses step-stress excitation rather than a constant excitation level**.** Thus, different components experience different loading histories based on their locations on the PWB and on the excitation history. For example, component U5 (SAC) failed under $10G_{rms}$ excitation, while component U2 (SAC) did not fail until the excitation was stepped up to $28G_{rms}$. The comparison of the durability for different components is difficult because of these different excitation histories. Thus an equivalent durability has to be calculated for each component to allow comparisons. This means that time to failure has to be normalized to some reference excitation level. The way to obtain this equivalent durability is by means of a durability scale factor. The concept of the durability scale factor is similar to that of the acceleration factor. In this study, the reference excitation level for the normalization is chosen to be $10G_{rms}$ (the lowest excitation level used in the test program).

The durability scale factor DSF_g at any excitation level G_{rms} is thus defined as:

$$DSF_g = \frac{\dot{D}_g}{\dot{D}_{10}} \tag{5}$$

Thus, the equivalent durability, $\hat{t}_{f_g}$ (time at excitation level G_{rms} converted to minutes at excitation level 10g) is:

$$\hat{t}_{f_g} = t_{f_g} * DSF_g \tag{6}$$

When there are multiple excitation levels, the total equivalent durability is obtained by summation of $\hat{t}_{f_g}$ at each level.

The durability scale factors, DSF_g depend on the component type, location on the PWB,

and excitation level, and are estimated from the FEA simulations, the measured strain histories, and the assumed fatigue constants, using Equations 1-5. For example, the DSF results for the BGA 225 component U4 are shown in Table 5 for both SAC and SnPb solders at the different excitation levels used in the JGPP test. The result shows that SnPb has a larger durability scale factor (larger acceleration factor for vibration testing) than SAC. The same scheme is applied to other component and calculates corresponding durability scale factors for all of them. With these durability scale factors, the equivalent durability for component U4 can be obtained (i.e. equivalent minutes at $10G_{rms}$ excitation). The process is repeated for all BGAs on the PWB and can be extended to other component types also.

Excitation (G_{rms})		10G	12G	14G	16G	18G	20G	28G
Durability scale factors for component U4	SnPb	1	4.26	11.09	21.14	27.63	45.12	434.21
	SAC	1	3.70	8.76	15.27	18.11	28.19	143.00

Table 5: Example of durability scale factors for BGA225 (eg. U4) for both SAC and SnPb

6. Durability Assessment for BGA225 Components

Failure test results for 10 BGA225 components are available from the JGPP study [10]. The locations of these10 BGA components are shown in Figure 1.

The equivalent durability for all BGA225 components are calculated based on the experimental durability (time to failure) results, the step-stress excitation history, and the durability scale factors, given in Table 5, as shown in Eqn 6. The results for SnPb and SAC are shown in Figures 12 and 13, respectively. The X-axis is the normalized number of cycles obtained by multiplying the equivalent durability (in seconds) by the frequency of the first mode. All the number-of-cycles to failure values are normalized to that of component U43 SAC. Thus, this conversion is most accurate for those interconnects where the fatigue damage is dominated by first mode deformation. Components with damage from second (or higher) modal deformations, will not scale very well for this plot. The Y-axis shows the cyclic strain range value that represents the threshold, above which 90% of the fatigue damage occurs at 10Grms.

The least square fit to the durability test data points for SnPb and SAC solders are also shown in Figures 12 and 13, on a log-log scale. The slope should agree reasonably well with the fatigue exponent for this failure mode. As shown in Figure 14, the data in this study spans across the nonlinear transition zone between the low-cycle fatigue (LCF) & high-cycle fatigue (HCF) regions of the fatigue curve. The best option therefore is to compare the slope of the least square fit to the test data with the secant slope of the fatigue curves over the test space as shown in Figure 14 and in Table 6. The fatigue curve presented in Figure 14 is based on the data given in Figure 11. The references for the data are given in Table 6.

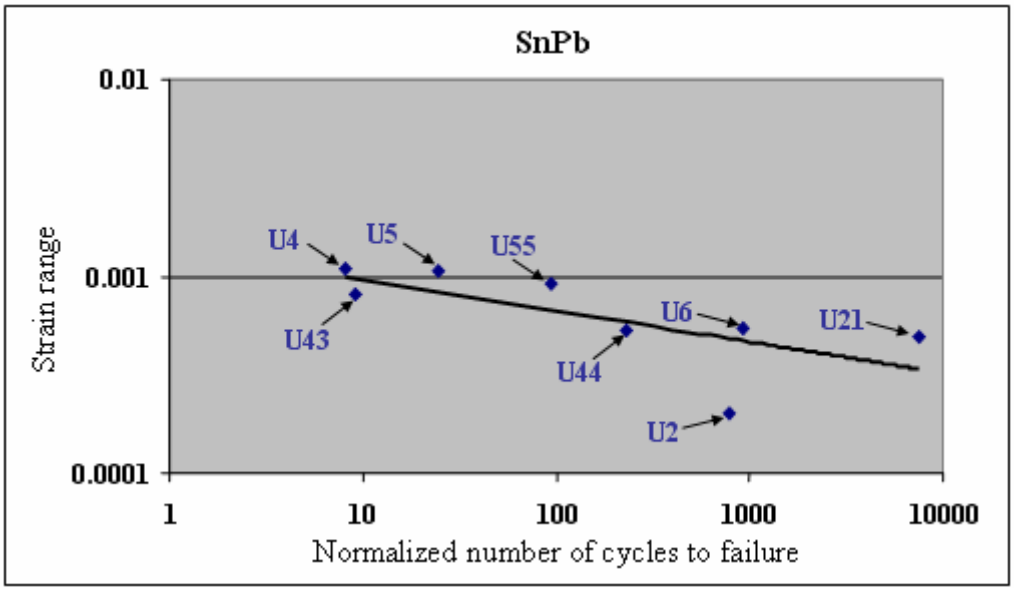

Figure 12: SnPb durability plot for BGA components (normalized with respect to the number of cycles to failure for component U43 SAC)

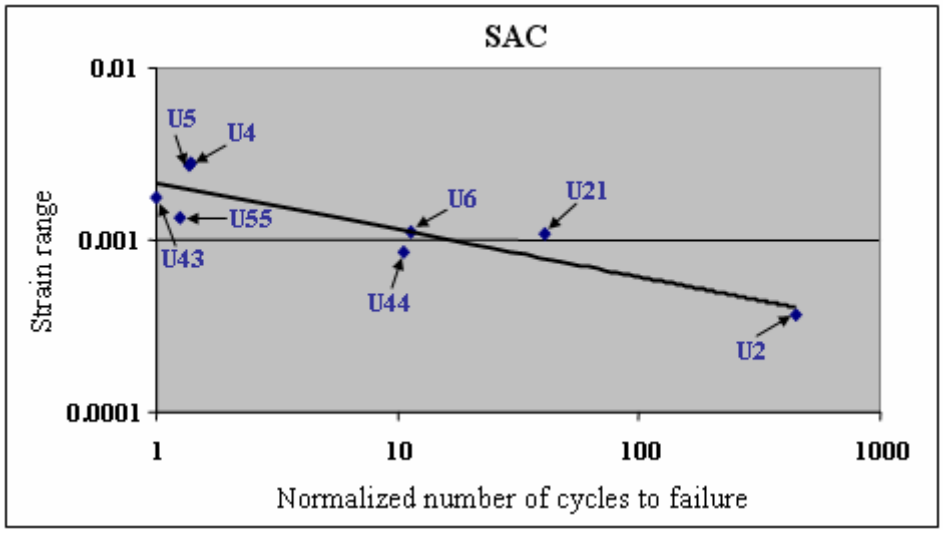

Figure 13: SAC durability plot for BGA components (normalized with respect to the number of cycles to failure for component U43 SAC)

This secant slope, as well as the slopes of the HCF (Basquin) curve and LCF (Coffin-Manson) curve, is listed in Table 6 for comparison to the test data. As seen from the table, the slope of the experimental data agrees approximately with the secant slope, thus providing some confidence in the fatigue exponents used in this study. Table 6 reveals that the exponents (slopes) used in the fatigue model are slightly smaller than the test data for SnPb and slightly larger than the test data for SAC. This discrepancy will impact the estimation of acceleration factors, as will be discussed later in Section 7. Furthermore, we find that although the LCF and HCF fatigue exponents match reasonably well with

the test data, the corresponding LCF & HCF fatigue coefficients do not match the test data well. For this reason, all the results in this study are presented with normalized scales so that the slopes (fatigue exponents) can be compared without having to compare the intercepts (fatigue coefficients). Further studies are in progress to obtain better estimates for the fatigue exponents and coefficients.

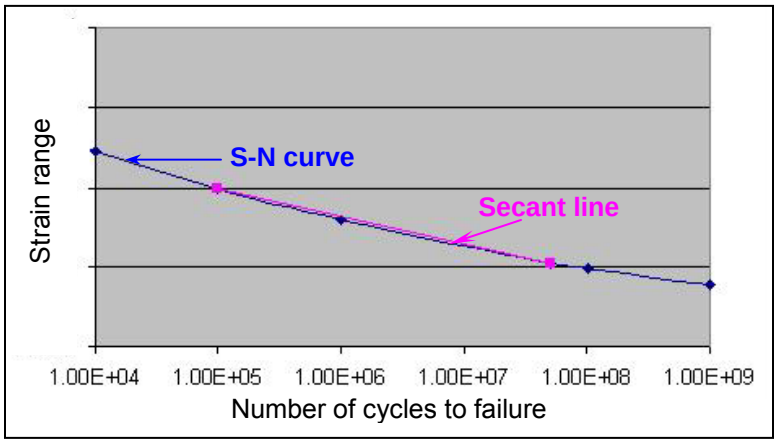

Figure 14: Secant slope for SAC from JGPP durability test data

	SnPb	SAC
Basquin exponent	-0.093 [15]	-0.11 [12]
Coffin-Manson exponent	-0.52 [15]	-0.49 [12]
Secant exponent	-0.13	-0.35
Experimental exponent	-0.158	-0.27

Table 6: Durability exponents from fatigue model and experimental data for SnPb and SAC solder

7. Results & Discussions:

Using the fatigue exponents validated in Section 6, it is now possible to use the scaling presented in Equations 1-6 to compare the relative ranking of the equivalent durability for all BGA225 components on the PWB as a function of the magnitude of PWB flexure (due to the location of the component on the PWB). Such a normalized plot is presented for both SAC and SnPb solders in Figure 15. The x-axis is the equivalent durability (cycles to failure converted to equivalent cycles at $10G_{rms}$). Similar normalization could have been done for any other excitation level. The durability data is normalized with respect to the durability of component U43 SAC, which failed first in the test. The y-axis shows the magnitude of the PWB flexure, normalized with respect to the highest PWB flexure, which is near component U55. The PWB flexure is the one-sigma value of the Gaussian response to the random excitation used in this study. This response magnitude was estimated with the global FEA described in Section 3 of this study. This plot provides a convenient way to demonstrate the reduction in vibration durability when making the transition from Sn37Pb to SAC solder.

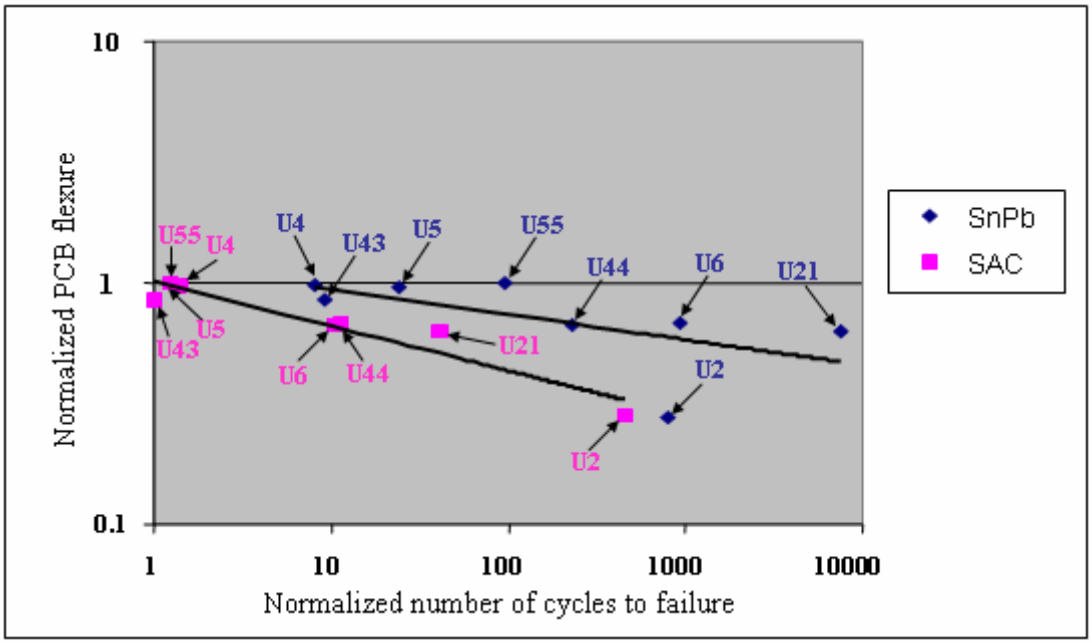

Figure 15: Normalized durability ranking for BGA225 components at various locations on the PWB test specimen

The other useful outcome of the fatigue exponents, validated in Section 6, is that acceleration factors can now be estimated for each component on the test specimen. These acceleration factors will allow us to extrapolate the failure data to other vibration levels encountered in testing or in service. As examples, the acceleration curves for component U2 are shown in Figure 16 for different levels of broad-band random excitation. At each loading level, the excitation bandwidth is held constant and the G_{RMS} is varied. In these plots, the y-axis is the excitation PSD level from 10G to 28G. The x-axis is the corresponding acceleration factor at each excitation level for both SAC and Sn37Pb solders. Acceleration factors are estimated relative to the durability at 28 G_{RMS} excitation. As expected from the secant slopes of the fatigue model, as well as from the slope of the test data (presented in Table 6), the acceleration factors are seen to be higher for Sn37Pb than for SAC. However, the difference between these two sets of acceleration factors is expected to be slightly less than the values presented in Figure 16, because of the discrepancies in slopes noted in Table 6 earlier.

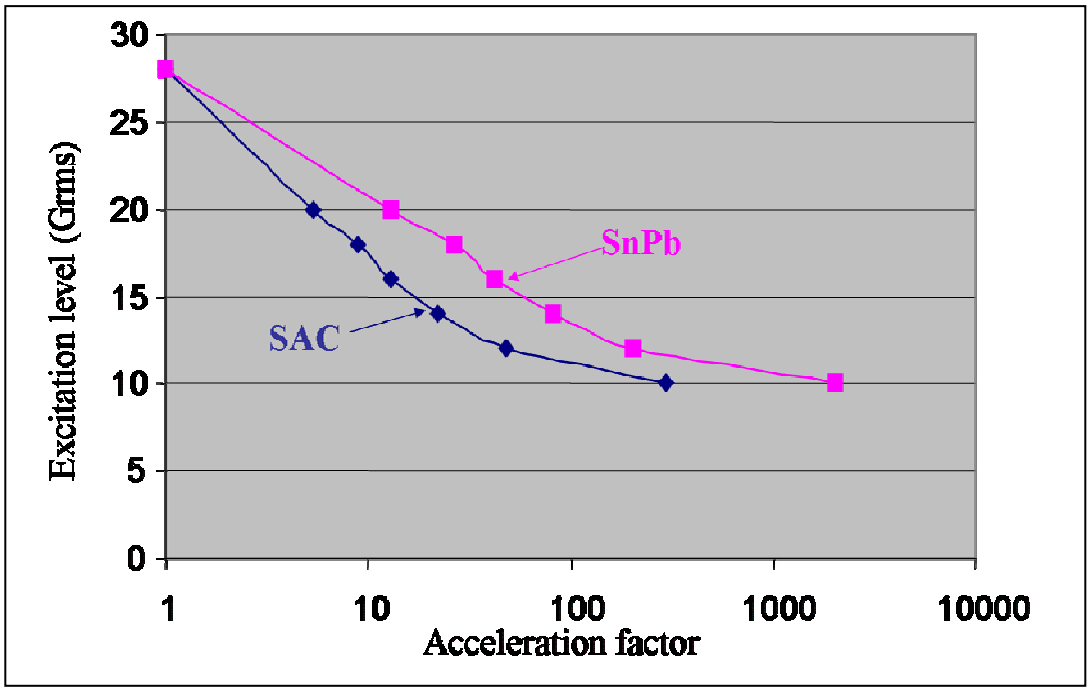

Figure 16: Acceleration factors for U2 (SAC & SnPb) at different excitation levels

8. SUMMARY and FUTURE WORK

The vibration durability of Sn37Pb and SAC solders has been compared, using combination of accelerated testing and physics-of-failure (PoF) modeling. The tests were conducted on selected surface mount components. The analysis has been conducted using a time-domain approach to quantity fatigue damage caused by broad-band, random, step-stress excitation. The analysis and damage modeling revealed that the slopes of the experimentally obtained durability plots agree reasonably well with the slopes of the HCF S-N curves of the solder materials. Further tests are needed to calibrate the intercept of the HCF S-N curves for both the SAC and SnPb materials. As a result of this study we were able to quantify the loss in vibration durability of the SAC BGA225 interconnects compared to their Sn37Pb counterparts on this test board. We were also able to quantify the corresponding decrease in acceleration factors for vibration testing of SAC solder system compared to their Sn37Pb counterpartsThese observations qualitatively agree with other published results. As an example, durability comparisons were provided in this report for 10 G_{RMS} excitation. Similar normalization could have been done for any other excitation level.

In this report, durability scale factors were based on fatigue exponents available in the literature for SAC and SnPb solders and the resulting prediction of time to failure was compared with test data. An alternate approach is to first estimate the secant fatigue exponent empirically by least-square fit to the test data and then comparing the resulting empirical durability scale factors with those estimated from literature data. This work is currently in progress and will be the subject of a future report.

Reference:

1. K. Darbha, S. Ling, A. Dasgupta, "Stress Analysis of Surface-Mount Interconnections Due to Vibration Loading", Journal of Electronic Packaging, Vol. 119, pp. 183-188, 1997
2. D. B. Barker and A. Dasgupta and M. G. Pecht, "PWB solder joint life calculation under thermal and vibration loading", Proceedings Annual Reliability and Maintainability Symposium, pp. 451-459, 1991
3. D. B. Barker, Y. S. Chen, and A. Dasgupta, "Estimating the vibration fatigue life of quad leaded surface mount components", Journal of Electronics packaging, vol. 115, pp. 195-200, 1993
4. S. Liguore, S. Fields, D. Followell, and R. Perez, "Vibration fatigue of leadless chip carrier solder joints", ASME paper 92-WA/EEP-25, 1992
5. J. Lau et al., "Solder joint reliability of surface mount connectors", Journal of Electronic Packaging, Vol. 115, pp. 180-188, 1993
6. J. Lau, "Solder joint reliability of flip chip and plastic ball grid array assemblies under thermal, mechanical and vibration conditions", IEEE Transactions on Components, Packaging, and Manufacturing Technology, Vol, 19, pp. 728-735, 1996
7. J. Lau, E. Schneider, and T. Baker, "Shock and vibration of solder bumped flip chip on organic coated copper boards", Journal of Electronics Packaging, Vol. 118, pp. 101-104, 1996
8. Q. J. Yang, Z. P. Wang, G. H. Lim, John H. L. Pang, F. F. Yap and R. M. Lin, "Reliability of PBGA Assemblies Under Out-of Plane Vibration Excitation", IEEE Transactions on Components and Packaging Technologies, Vol. 25, pp. 293-300, 2002
9. F. X. Che, H. L. J. Pang, F. L. Wong, G. H. Lim and T. H. Low, "Vibration Fatigue Test and Analysis for Flip Chip Solder Joints", Electronics Packaging Technology Conference, pp. 107-113, 2003
10. T. Woodrow, "JCAA/JG-PP Lead-Free Solder Project: Vibration Test", Boeing Electronics Materials and Processes Report - 582, Revision A, January 9, 2006
11. K. Upadhyayula and A. Dasgupta, "Physics-of-failure guidelines for accelerated qualification of electronic systems," Quality and Reliability Engineering International, Volume 14, Issue 6 , pp. 433 – 447, 1998
12. Q. Zhang, A. Dasgupta and P. Haswell "Isothermal Mechanical Durability of Three Selected PB-Free Solders: Sn3.9An0.6Cu, Sn3.5Ag and Sn0.7Cu", ASME, Vol. 127, pp. 512-522, 2005
13. R. Darveaux and K. Banerji "Constitutive Relations for Tin-Based Solder Joint", IEEE Transaction on components, Hybrid and Manufacturing Technology, vol. 15, No. 6, pp 1013-1023, 1992

14. N. E. Dowling, “Mechanical Behavior of Material: Engineering Methods for Deformation, Fracture, and Fatigue” Prentice-Hall,1999

15. K Upadhyayula, “An Incremental Damage Superposition Approach for Surface Mount Electronic Interconnect Durability under Combined Temperature and Vibration Environments”, Ph.D. Thesis, University of Maryland, 1999